QuEST
BORN TO ENGINEER

delamination damage analysis of curved composites subjected to compressive load using cohesive zone modelling

Composites are an integral part of structural design of Aerospace, Automotive, Marine, Construction, Manufacturing, etc.

Dr. Raju
QuEST Global

contents

Abstract

Composites are an integral part of structural design of Aerospace, Automotive, Marine, Construction, Manufacturing, etc. Composites are preferred for their added advantages over the metals such as high strength to weight ratio, directional strength, low electromagnetic signature, etc. However, their failure behaviour is more complex due to the alignment of the fibres in the loading direction where off-axis loading could also occur. This becomes much more complicated if the structure is of a curved shape.

Failure analysis of a curved L-bend subjected to compressive loads is focussed in the current study. Delamination onset and progression in Glass fibre reinforced polymer (GFRP) composite is investigated. During loading, internal layers (before the neutral axis) are subjected to compression and outer layers in tension. Delaminations reduce compressive strength of composite laminates as they allow out of plane displacement of plies to occur more easily. Delamination in the laminate occurs predominantly due to interlaminar tensile stresses.

Compressive out-of-plane loading induces subtle delaminations. Such damage may exponentially decrease structural integrity, yet can be difficult to detect. A 3-D FE analysis is performed to determine the stress distribution, location of delamination initiation and damage progression using MSC MARC FE package. Failure initiation is predicted using stress based failure criteria. Strain energy release rates and critical crack opening displacements are used to simulate crack growth using fracture mechanics. Interface elements are introduced at delamination sites. Ultimate failure loads are also predicted with the out-of-plane loading condition. The interlaminar stress distribution around the bend at the time of failure is determined.

Introduction

Layered composites allow the manufacture of structures with complex shapes and sizes. These complex structures generally consist of curved segments, which may enhance efficiency but generally involves complex failure mechanisms. Premature failures of curved composites occurred in the past were predominantly due to a lack of appreciation of interlaminar tensile strength. The primary failure mode in curved composites occurs when bends are opened or closed by external loading or pressure, as shown in Figure 1.

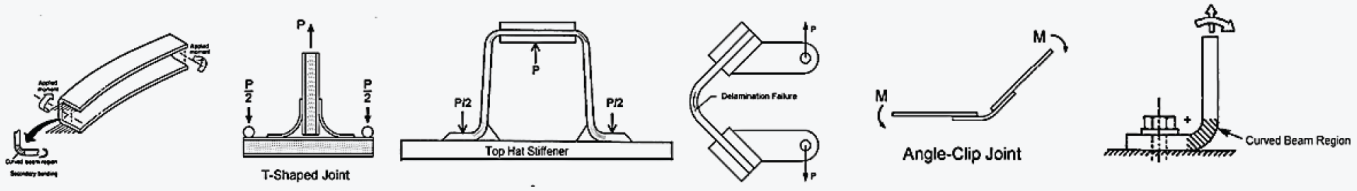

Figure 1: Curved structures inducing interlaminar tensile/compressive stress [Kedward et al., 1989]

Interlaminar tensile and compressive stresses generally develop when curved composite laminates are subjected to tensile or compressive loading in the plane of curvature [Kedward et al., 1989]. When curved composites are subjected to inward bending loads, inner surface tends to compress, generating circumferential compressive stress, whereas outer surface tends to expand, creating circumferential tensile stress. For design accuracy and failure prediction, it is essential to understand the interlaminar stress (tensile/compressive/shear) distribution during design and analysis of curved composite structures. The interlaminar tensile stress is a function of basic laminate constituents, such as type of reinforcement and matrix, stacking sequence, manufacturing process, fabrication quality, aging and type of loading, environmental degradation [Heinz et al., 2000;]. The stress distribution is complex in curved composites; they more often delaminate due to lack of through-thickness strength. A study of interlaminar stress distribution at the bends acts as a tool for understanding and predicting structural delamination. In the laminate, interlaminar tensile/compressive stress range is minimum at inner and outer surfaces and maximum at mid-thickness of the composite laminate.

Kedward et al. [1989] studied radial stress distribution for a curved beam using classic elastic theory. They simplified the strength of materials approach and conducted finite element analysis (FEA) using Nastran 2D and 3D elements. A finite element (FE) code was developed [Graff, 1989] to obtain stresses and strains in curved composite strap laminates (Graphite-Epoxy, Kevlar-Epoxy, Glass-Epoxy) numerically using Tsai-Wu failure criterion. Chang and Springer [1986] developed numerical codes to calculate interlaminar stress in a simple right angle bend subjected to pure moment. In-plane failure strength was predicted using Tsai-Hill failure criterion and out-of-plane strength using the Chang-Springer failure criterion. Later, comparisons between fracture-mechanics and strength-based delamination predictions were made [Martin and Jackson, 1993]. The difficulty of interlaminar tensile/compressive or shear stresses was highlighted at the bonded joints and attachments of marine composite structures [Dodkins and Shenoi, 1994]. Wisnom [1996] was one of the primary investigators, studying delamination failure through experimental, analytical and numerical approaches to detect interlaminar failure and determine flexural strength of composite laminates. Lekhnitskii's equations are applicable only for pure bending or edge loading; thus, they cannot sustain circumferential force without radial restraints. Shenoi and Wang [2001] developed equations based on elasticity theory for delamination and flexural strength of curved composites. The effects of key variables, such as stacking sequence and radius of curvature on stress distribution within a curved layered beam and sandwich beam were also studied. Among the different failure modes of composite materials, delamination mode predominates for curved laminates. Also failure analysis becomes more critical when the load is transferred in an out-of-plane mode.

One of the key challenges in designing composite structures is the high-strength joints. Often, the load needs to be transferred in an out-of-plane mode; joints carrying such loads must be carefully designed. Out-of-plane joints are formed by placing additional composite layers on both sides of the structure and filling the gap with an appropriate filler material. Generally used out-of-plane joints are the L-Bends, T-joints flanges of top-hat-stiffeners and other shapes as shown in the Figure 2.

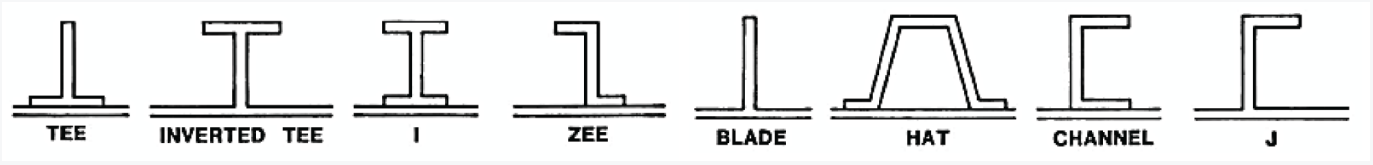

Figure 2: General out-of-Plane joint types

Composite Failure

Despite their numerous advantages, composite structural applications may pose a serious risk if the load-transfer and damage mechanisms are not properly analysed. Structural components are subjected to multiple loadings such as tension, compression, shear and flexure. The increase in the number of composite structure applications also demand in-depth study of the process of load transfer between the fibre and matrix at microscopic level to large delamination failures at the macroscopic level. Stress distribution and failure modes in composites are complex in nature. Geometric and material non-linearity complicates composite failure prediction; however, a fundamental feature of composite structures is that the failure is not usually a unique event, but an accumulation of a gradual sequence of micro cracking and delaminations leading to structural collapse [Hinton et al., 2004].

This could be overcome by better understanding of material properties, which may lead to reduced factor of safety, lower costs, lighter structures, superior design and lower potential hazards. Unlike metals, composites are brittle, and the possible failure parameters are matrix failure, fibre failure, interface failure and interlaminar failure. Commonly occurring defects in composite materials are presented in Table 1.

Matrix damage: Cracking	Creep
Matrix damage: Crazing	Crushing
Matrix damage: Incorrect cure	Cuts and scratches
Matrix damage: Moisture pick-up	Dents
Matrix damage: Porosity	Incorrect fibre volume ratio
Fibre damage: Broken	Incorrect materials
Fibre damage: Fibre/matrix debonding	Marcelled fibres
Fibre damage: Misalignment	Mismatched parts
Fibre damage: Miscollination	Missing plies
Fibre damage: Uneven distribution	Overaged prepreg
Fibre damage: Wrinkles or kinks	Over-/undercured
Delamination: Bearing surface damage	Ply underlap or gap
Delamination: Blistering	Prepreg variability
Delamination: Contamination	Reworked areas
Delamination: Corner radius delamination	Surface damage
Delamination: Corner/edge splitting	Surface oxidation
Delamination: Edge damage	Thermal stresses
Delamination: Fastener holes	Translaminar cracks
Delamination: Fibre/matrix debond	Variation in density
Delamination: Holes and penetration	Variation in thickness
Delamination: Fills or fuzz balls	Variation in resin fraction
Delamination: Surface Swelling	Missing Plies
Barely visible impact damage (BVID)	Erosion
Contamination of bonded surfaces	Voids
Corner cracking	Warping

Table 1: Types of defects found in composite materials [Heslehurst and Scott, 1990]

Interlaminar Failure - Delamination

Delamination is the primary failure mode in composites which reduces the strength and integrity of the structure, particularly through matrix cracking [Sridharan, 2008]. Delamination is induced by interlaminar tension and shear due to inherent factors such as stiffness (elastic modulus) mismatch between layers, structural discontinuities, free edge effects around holes, impact by a foreign object and through-thickness stress in curved composites. External factors such as fatigue, moisture and temperature variation and voids may also cause delamination. Other failure modes, such as matrix cracking, can also induce delamination. Most common sources of delamination in structural composites are material and structural discontinuities, as shown in Figure 3.

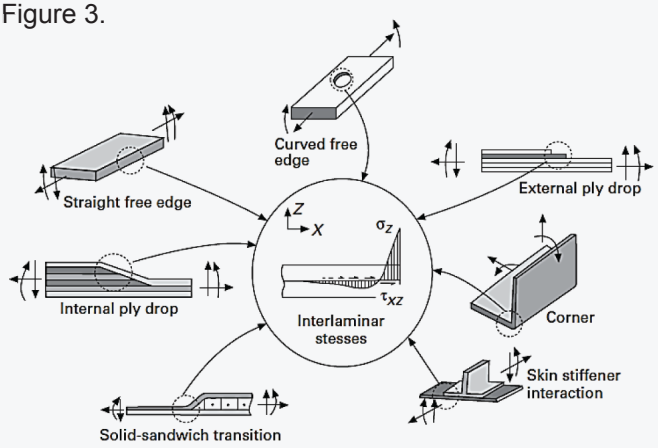

Figure 3: Delamination sources—material and geometric discontinuities [Sridharan, 2008]

Initial failure through delamination can be undetected, as delamination is frequently embedded between layers within the composite structure. In some cases, delamination may reduce residual strength of the structure as much as 60 per cent. The interlaminar tensile and shear stresses are the key parameters in defining delamination strength of the composite. However, these are matrix-related properties; it is very difficult to increase the delamination strength of the specimen without external fastenings. Many methods have been suggested for arresting interlaminar failure, such as using tougher matrix polymers, interleaf layers, through-thickness reinforcement, improved fibre/matrix strength and optimisation of fabrication, 3D weaving, Braiding, etc.

Delamination Prediction in Composites Using Numerical Methods

The different methods of predicting delamination failure are stress, fracture-mechanics, a combination of stress and fracture-mechanics, cohesive zone and strain invariants are discussed.

Stress-based Numerical Methods

Stress-based methods are efficient in predicting the initiation or onset of delamination in composite materials. Widely used failure

stress-based criteria are Puck, Grant-Sanders, Choi, Kim and Soni and Ye [Raju et al. 2013]. With these methods, stresses are compared

to the allowable stress of the structure to determine when delamination has occurred in each load increment. The basic form of delamination failure theory is

$$\frac{\sigma_{33}}{Z_t} \geq 1$$ *(Equation 1)*

Where Zt is the through-thickness tensile strength. Hou et al. [2001] studied the effect of shear stress distribution on delamination of the structure when the structure was subjected to compressive load. The out-of-plane tension accelerated the development of delamination, while out-of-plane compression limited delamination initiation.

Hou's theory suggests that the critical shear stress required to initiate delamination is much higher when the laminate experiences through-thickness compression. Shear delamination is eliminated altogether if the compressive load exceeds a critical value.

$$\text{For tensile delamination } (\sigma_{33} \geq 0), \left(\frac{\sigma_{33}}{Z_t}\right)^2 + \left(\frac{\sigma_{23}^2 + \sigma_{13}^2}{S_t}\right) \geq 1$$

$$\text{For compressive delamination } \left(\left\{\sqrt{\frac{\sigma_{13}^2 + \sigma_{23}^2}{8}}\right\} \leq \sigma_{33} < 0\right), \frac{\sigma_{13}^2 + \sigma_{23}^2 - 8\sigma_{33}^2}{S_t} \geq 1$$

$$\text{and No delamination when } \sigma_{33} < -\left(\sqrt{\frac{\sigma_{13}^2+\sigma_{23}^2}{8}}\right)$$ *(Equation 2)*

Ye [1988] proposed a failure criterion for delamination based on the interaction between the normal and shear through-thickness stresses.

$$\text{Tensile delamination } (\sigma_{33} \geq 0): \left(\frac{\sigma_{33}}{Z_t}\right)^2 + \left(\frac{\sigma_{13}}{S}\right)^2 + \left(\frac{\sigma_{23}}{S_t}\right)^2 \geq 1$$

$$\text{Compressive delamination } (\sigma_{33} < 0): \left(\frac{\sigma_{13}}{S}\right)^2 + \left(\frac{\sigma_{23}}{S}\right)^2 \geq 1$$

Zhang [1998] modified Ye's criteria into tensile- and shear-failure modes.

$$\text{Tensile mode: } \left(\frac{\sigma_{33}}{Z_t}\right) \geq 1$$

$$\text{Shear mode: } \left(\frac{\sigma_{13}^2+\sigma_{23}^2}{S_t}\right) \geq 1$$ *(Equation 3)*

Where Zt = through-thickness tensile strength; S = in-plane shear strength; St = interlaminar shear strength.

Although stress-based methods determine crack initiation, they require a finer mesh in the through-thickness direction to account for a complex stress field. Moreover, it is difficult to model the crack progression using stress-based methods due to their high stresses at the crack tip.

Fracture-Mechanics-based Numerical Modelling

Numerical methods based on LEFM have proven effective in predicting delamination growth in composites; however, these methods require the pre-existence of an initial crack front. Once a crack occurs, delamination growth is achieved when the combination of the components of energy release rate is equal to or greater than a critical value. Various methods have been used to obtain the delamination growth, such as the virtual crack-closure technique (VCCT), cohesive zone modelling and J-integral.

The mostly widely employed delamination criteria is the VCCT [Rybicky and Kanninen, 1977], which is an extension to finite element analysis (FEA) of Irwin's crack-closure integral. The technique is based on the assumption that the energy released during crack propagation is the same as the energy required closing the crack. VCCT is applicable for both shell and solid models based on the strain energy release rate (SERR). However, the main drawback of VCCT is the requirement of the pre-existence of a crack front. The major difficulty in the study of a failure using VCCT is the mesh dependency in the stress-based methods, particularly when delamination is present. The fracture-mechanics approaches rely on the definition of an initial flaw or crack; however, in a practical situation, the location of damage initiation is not obvious. Therefore, stress-based methods can be used to predict the onset of delamination and fracturemechanics provides accurate delamination propagation modelling.

Cohesive damage models have been developed based on damage mechanics to simulate the onset and growth of fractures/cracks. They do not depend on a predefined crack/defect. The cohesive elements combine the aspects of strength-based analysis to predict the onset of damage at the interface and fracture-mechanics to predict the propagation of delamination. Interface elements are separate FE entities modelled between the substructures of a composite material as a means of inserting a damageable layer for delamination modelling. Interface elements can be modelled in various ways, from nodal 2D spring connections [Cui et al., 1993;] to full 3D solid element formulations [Goyal et al., 2004;]. These elements are designed to represent the separation at the zero-thickness interface between the layers of 3D elements during delamination. In addition, these elements are sufficiently stiff in compression to prevent interpenetration of the delaminated surfaces. The main advantage of using cohesive elements is its ability to predict both onset and propagation of delamination without previous knowledge of the crack location and propagation direction. However, it is limited to a very fine mesh and can produce unacceptably inaccurate predictions when large sized elements are employed. According to Turon et al. [2007], the cohesive element is an efficient approach to model a fracture when the crack propagation is known a priori.

Strain - Invariant Failure Theory (SIFT)

Gosse and Christensen [2001] proposed a micromechanical 3D strain-based approach to predict failures in composites, called the strain-invariant failure theory (SIFT). Strain tensors extracted from experiments are substituted into strain invariant parameters of J1 (first invariant of strain) and εvm (von Mises strain). The critical properties required for this theory are the critical first invariant of strain and the critical equivalent strain for both the matrix and fibre reinforcement phases.

$$J_1 = \varepsilon_1 + \varepsilon_2 + \varepsilon_3 \quad \textit{(Equation 4)}$$

$$\varepsilon_{vm} = \sqrt{\frac{1}{2}[(\varepsilon_1 - \varepsilon_2)^2 + (\varepsilon_2 - \varepsilon_3)^2 + (\varepsilon_3 - \varepsilon_1)^2] + \frac{3}{4}[\gamma_{12}^2 + \gamma_{23}^2 + \gamma_{31}^2]} \quad \textit{(Equation 5)}$$

Failure occurs at either the fibre or the matrix phase when any of these invariants first exceeds the critical values.

In the current study, preliminary FE modelling is carried out for L-bend composites to understand the interlaminar tensile stress (ILTS) and interlaminar shear stress (ILSS) distribution and failure. Failure location and mode were identified and successfully modelled for the L-bend composites.

L-bend Laminates

Non-linear static analysis is conducted on L-bend curved composite specimens subjected to compressive load. The failure modelling is based on the ILTS and ILSS distributions. The curved beam is subjected to pure bending such that the angle of the bend is decreased (i.e., the bend is closed). The maximum ILTS occurs within the thickness of the laminate and minimum at the outer surfaces.

Specimen geometry and laminate stack-up sequence

The geometry of the L-bend specimen is shown in Figure 4. Two boundary conditions are used; all nodes at the base are fixed and the loading node is subjected to a maximum displacement of 100 mm.

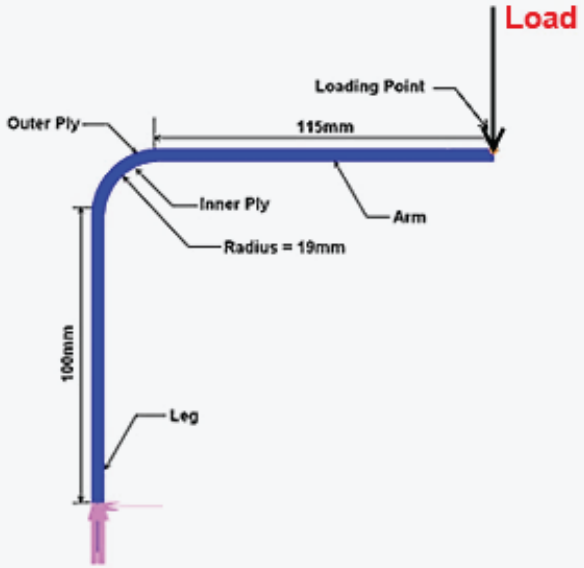

Figure 4: FE model of L-bend

The laminate is loaded with a point load at the tip of the arm as shown in Figure 4. Each element thickness represents the thickness of one layer in the composite laminate, except the first layer, which has three elements in the through-thickness direction to increase the ILTS accuracy at the inner surface. A static load case was defined with 100 fixed load steps. The study was carried out on the three different layups described in Table 2.

Three different glass fibre mats were used in the study. Two different weights of chopped strand mat (CSM) (450 and 225 gsm), double bias (DB ±45) 461 gsm, unidirectional (UD) 450 gsm and biaxial (BE) 450 gsm were used. The material properties of chopped strand mat, double bias and unidirectional fibres manufactured by hand-layup are presented in Table 3.

Layers	Layup 1 - CSM	Layup 2 - CSM+DB	Layup 3 - CSM+DB+UD
Layer 1	CSM 450gsm	CSM 450gsm	DB 611gsm
Layer 2	CSM 450gsm	DB 611gsm	CSM 450gsm
Layer 3	CSM 450gsm	CSM 450gsm	UD 451gsm
Layer 4	CSM 450gsm	DB 611gsm	DB 611gsm
Layer 5	CSM 450gsm	CSM 450gsm	CSM 450gsm
Layer 6	CSM 450gsm	DB 611gsm	UD451gsm
Layer 7	CSM 450gsm	CSM 450gsm	DB 611gsm
Thickness	4.62mm	4.62mm	4.62mm

Table 2: Layup configuration for L-bend laminates

Hand - layup Material Properties			
Property	**CMS**	**DB**	**UD**
E_{11} (MPa)[b]	9607	7872	23576
E_{22} (MPa)[b]	9607	7872	6560
E_{33} (MPa)[c]	6062	6673	6560
υ_{12} (MPa) [c]	0.347	0.62	0.369
υ_{23} (MPa) [c]	0.139	0.146	0.249
υ_{31} (MPa) [c]	0.108	0.133	0.087
G_{12} (MPa) [c]	2602	7157	2265
G_{23} (MPa) [c]	1847	2050	1847
G_{31} (MPa) [c]	1847	2050	2265
ILTS (MPa)[a]	9.5	10.5	10.5
ILSS (MPa)[a]	28	30	28
Flexure Modulus (MPa)[b]	1822	1169	4235
Flexure Strength (MPa)[b]	222	75	437
Fracture Toughness G1C (kJ/m^2)[a]	0.68	1.04	0.84
Critical opening displacement (mm)[A]	0.05	0.05	0.05

[a] Literature [Johnson, 1986; Dirand et al., 1996]
[b] Experimental testing
[c] Using 'Component Design and Analysis (CoDA)' software with resin and fibre properties

Table 3: Material properties–hand-layup process

FE Model Definition

The current study is being done using MSC MARC v2012. Eight-node isoparametric hexahedral elements (element type 7 of MSC MARC) were used with geometric and material non-linearity. These brick elements allow the definition of layer-by-layer material parameters, layer thickness, and orientation angles for a laminated composite material. A finer mesh with a global edge length of 1 mm was used around the bend (crown-web interface) to increase the number of elements in the complex geometry. The assumed strain formulation was also triggered to improve the bending accuracy for the 3D element. All the elements were modelled with local co-ordinate system.

Failure Modelling

The FE software has a built-in progressive failure capability, with or without element elimination and stiffness reduction, using various failure criteria such as Hoffman, Tsai-Wu, Tsai-Hill, Hashin, Puck and the maximum stress criterion. The primary mode of failure in curved composites is delamination, which is caused by the interaction of interlaminar tensile (σr) and shear (τrθ) stresses. The key aim of this study is to better understand the variation of radial (ILTS) and tangential (ILSS) stresses resulting from laminate curvature, stacking sequence and fibre orientation in curved composite structures. Thus, in the current model, interface elements are used to simulate the onset and progress of delamination. The constitutive behaviour of these interface elements is expressed in terms of traction vs. displacement between the top and bottom edge/surface of the elements (Figure 5).

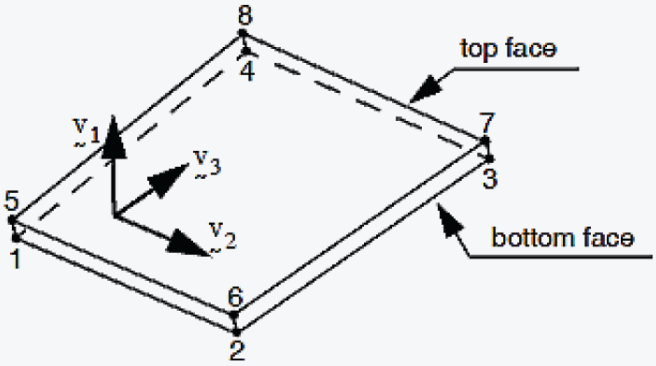

Figure 5: 3D linear interface element
[MSC MARC Volume A, 2012]

Element 188 in MSC MARC MENTAT 2008r1 is designed for a cohesive zone element, which is a linear, eight-node, 3D element typically used to model the interface between different materials, where nodes 1, 2, 3 and 4 correspond to the bottom of the interface and nodes 5, 6, 7 and 8 to the top. The stress components of the element are one normal traction and two shear tractions, which are expressed with respect to local coordinate system; corresponding deformations are the relative displacements between the top and bottom face of the element. The element is allowed to be infinitely thin, in which case faces 1-2-3-4 and 5-6-7-8 coincide.

For a 3D interface element, the relative displacement components are given by one normal and two shear components, expressed with respect to local element co-ordinate system as shown in Equation 6.

$$v_n = u_1^{top} - u_1^{bottom}$$
$$v_s = u_2^{top} - u_2^{bottom}$$
$$v_t = u_3^{top} - u_3^{bottom}$$

(Equation 6)

Based on the relative displacement components, the effective opening displacement is defined in Equation 7:

$$v = \sqrt{v_n^2 + v_s^2 + v_t^2}$$

(Equation 7)

Damage onset is predicted using a quadratic stress criterion, allowing the mesh to split between the materials using Equation 8.

$$\left(\frac{\sigma_t}{S_t}\right)^2 + \left(\frac{\sigma_s}{S_s}\right)^2 = 1$$

(Equation 8)

Where, σ_t and σ_s are the normal and tangential stresses and S_t and S_s, are the critical values of normal and tangential stresses. Typical interlaminar strength values for the reinforcements used, are given in Table 3.

The traction-separation model assumes linear elastic behaviour, written in terms of an elastic constitutive tensor 'K' relating the nominal stresses (traction vector) t=(t_n, t_s, t_t) to the nominal strains (opening displacement vector) v(v_n, v_s, v_t) across the interface. The effective traction is introduced as a function of the effective opening displacement and characterised by an initial reversible response, followed by an irreversible response as soon as a critical effective opening displacement has been reached, as shown in Figure 6. The irreversible part is characterised by increasing damage, ranging from zero (onset of delamination) to one (full delamination).

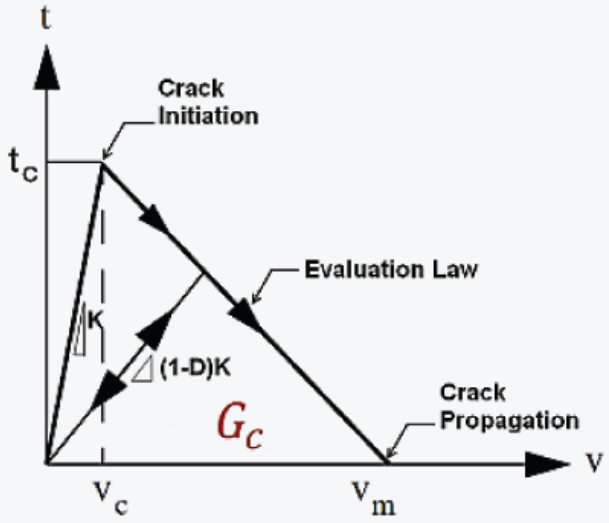

Figure 6: Damage evolution curve for bilinear cohesive element [MSC MARC Volume A, 2012]

For maximum effective traction, tc corresponding to the critical effective opening displacement vc is expressed in Equation 9.

$$t_c = \frac{2G_c}{v_m} \qquad \textit{(Equation 9)}$$

Once the corresponding initiation criterion is reached, the specified damage evolution law describes the rate the material stiffness degrades. A scalar damage variable 'D' represents the overall damage in the material and captures the combined effects of all active degradation mechanisms. In the current model, a bilinear model is used to obtain the traction 't'. When the overall damage variable reaches its limit 'D_{max}' at all material points, the cohesive element corresponding to complete fracture of the interface between layers can be removed and is considered as delamination propagation.

Results and Discussion

The curved laminates were loaded such that the radius of curvature contracted and interlaminar compressive stresses were induced in the inner surface. The load was applied to push the arm of the specimen, bending it. The peak ILTS occurs in the middle of the width of the specimen as the loading point is there. Through-thickness ILTS was maximum at the lower end of the radius of the bend and this location was predicted as the probable location of initial failure. For all three layups, interlaminar matrix cracking occurred due to excessive ILTS and delamination initiated at the lower end of the bend. The critical interlaminar tensile and shear stresses of the three layups are presented in Figures 8 and 9. The theoretical ILTS on the extreme surface is zero; however, due to positioning of the Gauss points, which do not sit on the surface of the elements, the interlaminar stress calculated at this point is a non-zero value.

The detailed load-deflection plot is shown in Figure 7. As expected, Layup-3 with UD laminates had higher stiffness. However due to mismatch in the stiffness between the layers (Layup 3), pre-mature failure occurred which could be seen around 930 N.

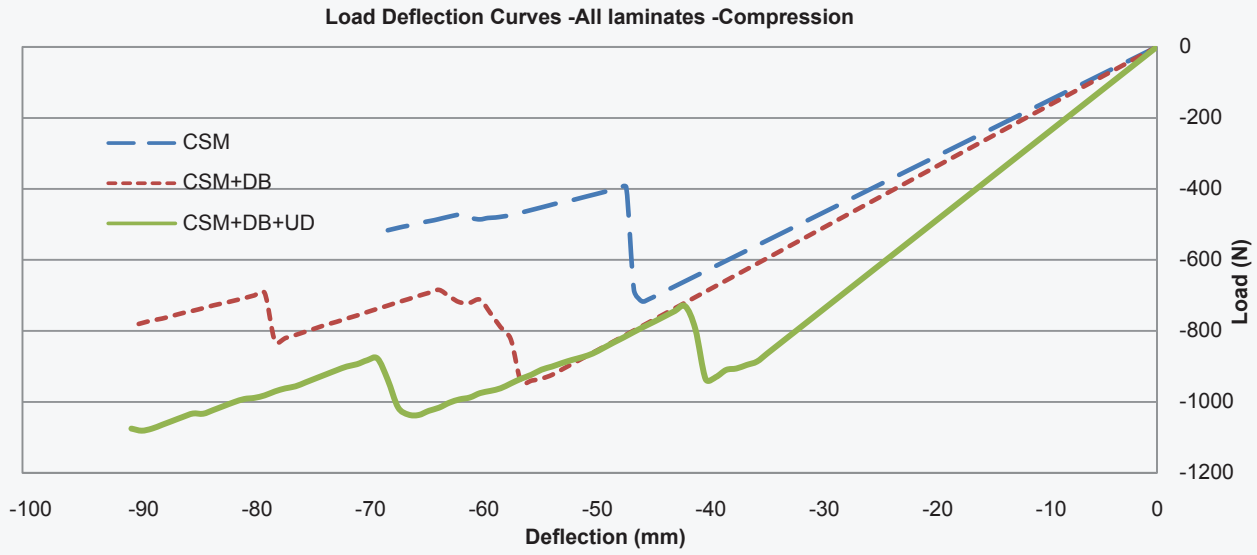

Figure 7: L-Bend FEA load-deflection plot for three different layups

Implicit FEA attempts to force convergence of loads or displacements, and this convergence becomes more complex and computationally expensive when the material becomes highly distorted and damaged. Yet, the MSC MARC MENTAT 2012 was able to predict the initial failure, as well the failure progression. The numerical model discussed in this section attempted to determine the regions of maximum interlaminar tensile and shear stress. The ILTS and ILSS plots for Layup 1 are presented in Figure 9. The ILTS distribution is comparable for all the three layups (Table 4); however, Layups 2 and 3 have higher ILSS values, which may be attributed to a mismatch in the elastic properties between adjacent layers.

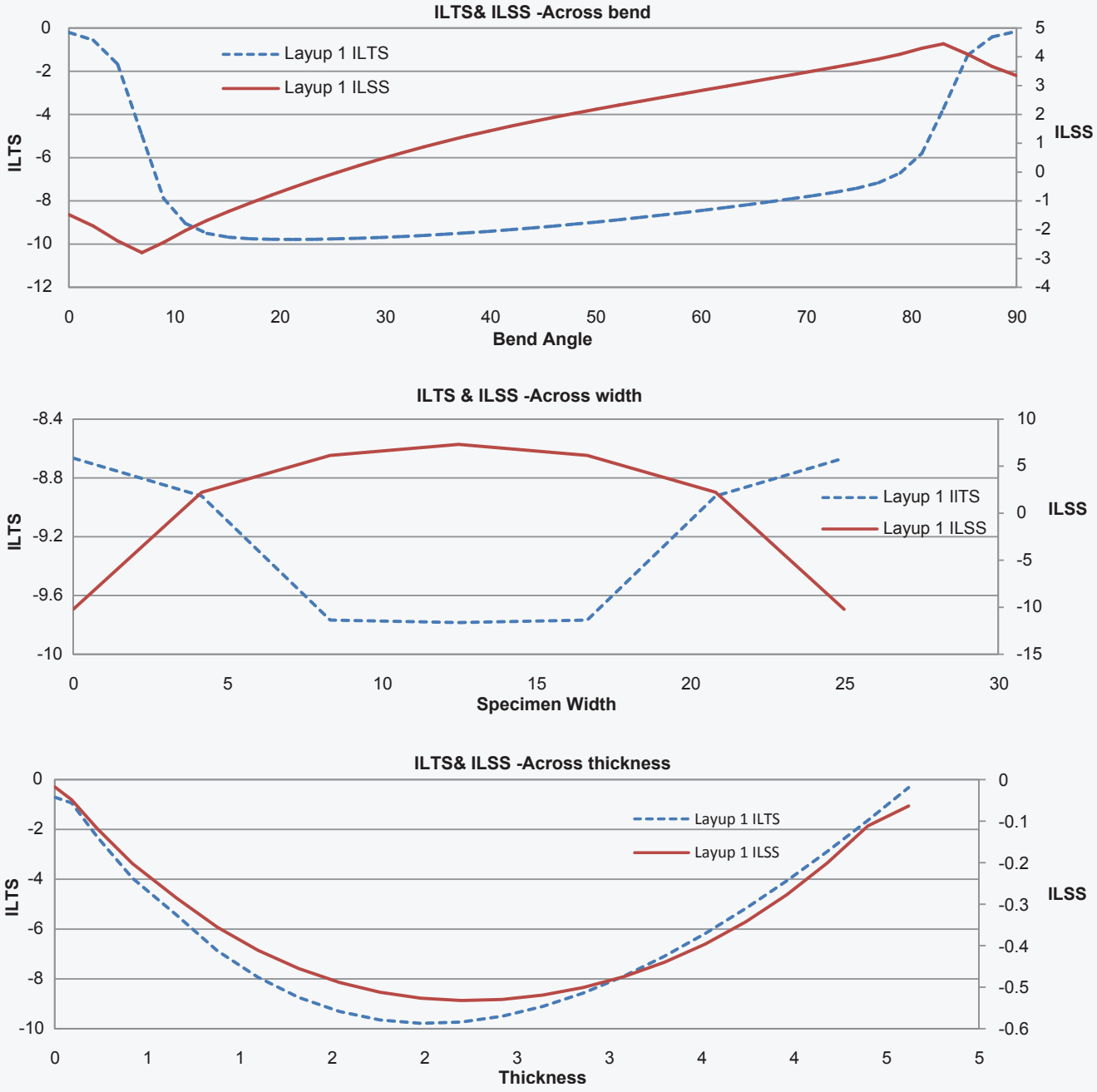

Figure 8: L-Bend ILTS & ILSS distribution just before first failure for Layup-1

L-Bend Layup 1 (All CSM) FEA results

All layers of the laminate in Layup 1 are CSM. The ILTS and ILSS stress distributions prior to the first failure are shown in Figure 9. The ILTS curve is smooth and linear until mid-thickness and drops to near zero at the surface, as shown in Figure 8. With this layup, the initial failure occurred at a displacement of 65 mm, predominantly due to interlaminar tensile stress of 9.22 MPa, between the third and fourth layers, mid-width and at an angle of 21.34°. The corresponding ILSS at the point was 0.53MPa. Further loading caused the laminate to straighten, creating ILTS in the inner surface and interlaminar compressive stress on the outer surface. Corresponding location and values of Interlaminar tensile and shear stresses for all the three layups are given in Table 4.

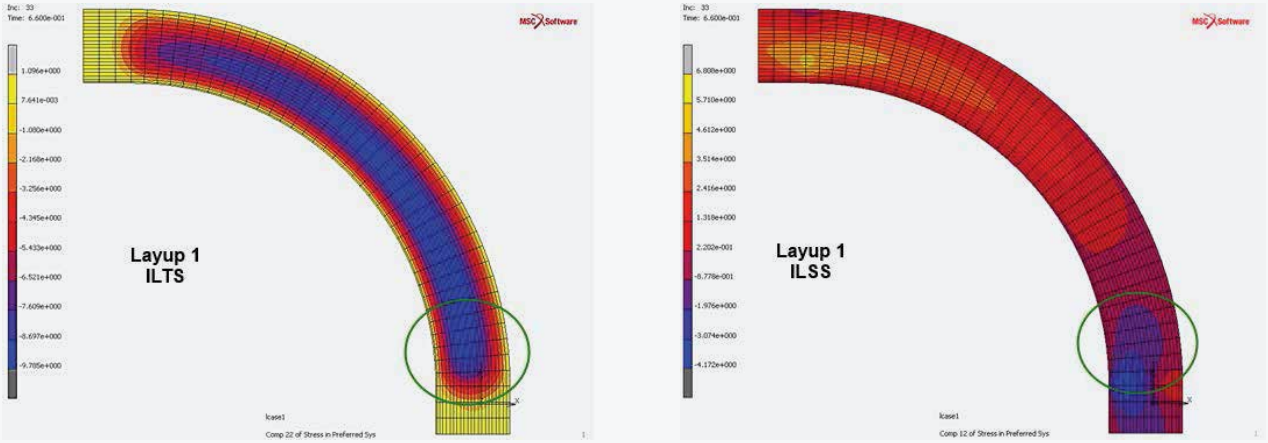

Figure 9: L-Bend Layup 1 ILTS and ILSS distribution

Layup	Deflection (mm)	ILTS (MPa)	ILSS (MPa)	Between Layers	Angle(deg)	Width (mm)
Layup 1	45.43	9.7847	0.5270	3 & 4	21.34	50
Layup 2	56.08	9.3778	0.7315	3 & 4	26.76	50
Layup 3	39.78	9.4620	0.9632	3 & 4	28.56	50

Table 4: Location and ILTS& ILSS values at First failure around the bend

Conclusion

L-bend Specimens of three different layups were analysed till failure under compressive load. The specimens were not loaded by pure moment; hence, the failures do not occur exactly at 45. The maximum ILSS for all three layups occurred at the lower end of the laminate bend. The failure criterion for FEA is a function of both the interlaminar tensile and shear stresses. Interlaminar tensile stress dominated the initial failures for all three layups. It is deduced that the accurate damage location and loading can be determined through the interaction of the interlaminar stresses.

References

1) Chang F.K., Springer G.S. (1986). The strengths of fibre reinforced composite bends. Journal of Composite Materials 20: 30-45.

2) Cui W.C., Wisnom M.R. (1993). A combined stress-based and fracture-mechanics-based model for predicting delamination in composites. Composites 24(6): 467-474.

3) Dirand X., Hilaire B., Soulier J.P. Nardin M. (1996). Interficial shear strength in glass-fiber/vinylester-resin composites. Composites Science and Technology 56: 533-539.

4) Dodkins A.R., Shenoi R.A., Hawkins G.L. (1994). Design of joints and attachments in FRP ship structures. Marine Structures 7: 364-398.

5) Gosse J.H., Christensen S. (2001). Strain invariant failure criteria for polymers in composite materials. AIAA-2001-1184, American Institute of Aeronautics and Astronautics, USA.

6) Goyal V.K., Jaunky N.R., Johnson E.R., Ambur D.R. (2004). Intralaminar and interlaminar progressive failure analyses of composite panels with circular cut-outs. Composite Structures 64(1): 91-105.

7) Graff E. (1989). Mechanical behaviour of thick curved laminated composites. PhD thesis, Stanford University.

8) Heinz. D., Ritcher B., Weber S. (2000). Application of advanced materials for ship construction – Experience and problems. Materials and Corrosion 51: 407-412.

9) Heslehurst R.B., Scott M. (1990). Review of defects and damage pertaining to composite aircraft components. Composite Polymers 3(2): 103-133.

10) Hinton M.J., Kaddour A.S., Soden P.D. (2004). Failure Criteria in Fibre Reinforced Polymer Composites. The World-Wide Failure Exercise. Elsevier Science Publishers.

11) Hou J.P., Petrinic N., Ruiz C. (2001). A delamination criterion for laminated composites under low-velocity impact. Composites Science and Technology 61(14): 2069-2074.

12) Johnson A.F. (1986). Comparison of the mechanical properties of SMC with laminated GRP materials. Composites 3: 233-239.

13) Kedward K.T., Wilson R.S., Mclean S.K. (1989). Flexure of simply curved composite shapes. Composites 20(6): 527-536.

14) Martin R.H., Jackson W.C. (1993). Damage Prediction in Cross-Plied curved composite laminates. Composite Materials. Fatigue and Fracture 4: 105-126.

15) MSC MARC® 2012 -Volume A (2012). Theory and User Information. MSC. Software Corporation, CA, USA.

16) Raju, Prusty B.G., Kelly D.W (2013). Delamination failure of composite top-hat stiffeners using finite element analysis. Proceedings of the Institution of Mechanical Engineers, Part M Journal of Engineering for the Maritime Environment, 227(1):61-80.

17) Rybicky E.F., Kanninen M.F. (1977). A finite element calculation of stress intensity factors by a modified crack closure integral. Engineering Fracture Mechanics 9(4): 931-938.

18) Shenoi R.A., Wang W. (2001). Through-thickness stresses in curved composite laminates and sandwich beams. Composites Science and Technology 61: 1501-1512.

19) Sridharan S. (2008). Delamination behaviour of composites. Boca Raton, FL: CRC Press, ISBN - 9-781420-079678.

20) Turon A., Da´vila C.G., Camanho P.P., Costa J. (2007). An engineering solution for mesh size effects in the simulation of delamination using cohesive zone models. Engineering Fracture Mechanics 74: 1665–1682.

21) Wisnom M.R. (1996). 3-D Finite element analysis of curved beams in bending. Journal of Composite Material 30(11): 1178–1190.

22) Ye L. (1988). Role of matrix resin in delamination onset and growth in composite laminates. Composites Science and Technology 33(4): 257-277.

23) Zhang X. (1998). Impact damage in composite aircraft structures-experimental testing and numerical simulation. Proceedings of the Institution of Mechanical Engineers, Part G: Journal of Aerospace Engineering 212(4): 245-259.

About QuEST Global

QuEST Global is a focused global engineering solutions provider with a proven track record of over 17 years serving the product development & production engineering needs of high technology companies. A pioneer in global engineering services, QuEST is a trusted, strategic and long term partner for many Fortune 500 companies in the Aero Engines, Aerospace & Defence, Transportation, Oil & Gas, Power, Healthcare and other high tech industries. The company offers mechanical, electrical, electronics, embedded, engineering software, engineering analytics, manufacturing engineering and supply chain transformative solutions across the complete engineering lifecycle.

QuEST partners with customers to continuously create value through customer-centric culture, continuous improvement mind-set, as well as domain specific engineering capability. Through its local-global model, QuEST provides maximum value engineering interactions locally, along with high quality deliveries at optimal cost from global locations. The company comprises of more than 7,000 passionate engineers of nine different nationalities intent on making a positive impact to the business of world class customers, transforming the way they do engineering.

QUEST

BORN TO ENGINEER

http://quest-global.com